




Theoretical description of thermodynamic and mechanical properties of multicomponent bcc Fe-Cr-based alloys

A. V. Ponomareva, M. P. Belov, E. A. Smirnova , K. V. Karavaev, K. Sidnov, B. O. Mukhamedov ,* and I. A. Abrikosov [†]
Materials Modeling and Development Laboratory, National University of Science and Technology "MISIS," Moscow 119049, Russia

 (Received 15 June 2020; revised 3 August 2020; accepted 27 August 2020; published 14 September 2020)

Fe-Cr-based steels are broadly considered as important structural materials, e.g., for generation-IV nuclear reactors. In order to address tougher operation conditions in future applications, properties of existing Fe-Cr-based steels must be significantly improved. Multicomponent alloying has been viewed as an efficient tool to achieve this goal. Despite its accepted importance, fundamental knowledge of the effect of the simultaneous alloying of Fe with Cr and other elements, such as Ni, Mo, Al, W, V, and Nb, on the thermodynamic and mechanical properties of the bcc alloys is still quite limited. Here we report results of first-principles simulations of lattice parameters, mixing enthalpies, and magnetic and elastic properties of bcc Fe-Cr-based solid solutions with up to 20% Ni, as well as with small concentrations of other alloying elements, Mo, Al, W, V, and Nb. We predict that alloys with relatively high Ni concentrations containing 2.5%–5% Al demonstrate a simultaneous increase of thermodynamic stability and ductility without significant drop of their elastic moduli with respect to corresponding binary Fe-Cr alloys.

DOI: [10.1103/PhysRevMaterials.4.094406](https://doi.org/10.1103/PhysRevMaterials.4.094406)

I. INTRODUCTION

Generation-IV nuclear reactors are viewed as an important component in addressing the challenge of reducing carbon dioxide emission. One of the key tasks in the development of the next generation of nuclear reactors is the selection of materials that can withstand extreme operating conditions and are resistant to accelerated degradation caused by fast neutron fluxes, high temperatures, or corrosion. Fe-Cr-based steels are perhaps the main candidates for applications as core materials and as structural materials for steam generators. Moreover, they are broadly considered as possible pressure vessel steels in different designs of the generation-IV reactors and as breeding blankets for fusion applications [1]. In order to address tougher operation conditions in future applications, properties of existing Fe-Cr-based steels must be significantly improved. Multicomponent alloying has been viewed as an efficient path to achieve this goal.

The experimental investigations of materials intended for nuclear energy applications is both challenging and expensive. Therefore a fundamental description of their behavior on an atomic scale is required for a successful and effective design. Reliable databases of thermodynamic, mechanical, and magnetic characteristics of these materials are also necessary. Accurate theoretical modeling of multicomponent Fe-Cr-based alloys would allow one to get information on the thermodynamic, magnetic, and elastic properties, which in turn should provide a conceptual framework of a knowledge-based design of the materials for applications in energy technologies. Indeed, first-principles calculations have been

actively used to study the Fe-Cr based alloys. Most of the theoretical works on phase equilibrium in Fe-Cr alloys [2–6] have indicated that chemical interactions arising from magnetism play a key role in their thermodynamic stability, including the anomalous stability of the Fe-rich bcc alloys.

The modeling of Fe-Cr alloys using the generalized perturbation method (GPM) and the tight-binding approximation predicted that for concentrations of about 25 at % Cr the effective pair interaction in the first coordination shell changed sign from positive to negative [7]. The negative sign indicated that clustering should take place for high-Cr alloys. Neutron diffraction measurements in Ref. [8] showed that clustering occurs at concentrations about 15 at % Cr. On the other hand, at low Cr concentrations a large and positive pair interaction in the first coordination shell indicated the possible existence of a chemical short-range order. Thus GPM modeling of the Fe-Cr alloys suggests that in the system effective pair interaction can change sign with concentration. Despite all the approximations used in the GPM model, the theoretical results on the effective interactions [7] appeared rather satisfactory and later were confirmed by neutron scattering measurements of atomic short-range order [9].

Density functional theory (DFT) calculations of the mixing enthalpy of ferromagnetic bcc Fe-Cr alloys confirmed the anomalous stability of the alloys with low Cr concentrations [2–5,10]: the mixing enthalpy was found to be negative at concentrations of Cr below 6 at %. At the same time it became positive for higher Cr concentrations and reached a maximum value of 10 kJ/mol for the equimolar composition. In addition, it was found that the bulk modulus, both theoretical and experimental, has a peculiarity at around the same concentration of 6 at % Cr [5]. Currently, most studies are consistent on the fact that the anomalous stability of diluted Fe-Cr alloys originates from the magnetic behavior of Cr atoms, which

*Corresponding author: muhamedov.b@misis.ru

[†]Corresponding author: abrikosov.ia@misis.ru

have an induced magnetic moment aligned antiparallel to the Fe magnetic moment due to antiferromagnetic exchange interactions. At the same time, the magnetic exchange interactions for Cr-Cr pairs in the first coordination shell are also antiferromagnetic. Thus the appearance of a pair of Cr atoms as the nearest neighbors leads to a frustration of the local magnetic configuration. As a result, with an increased Cr concentration its magnetic moment gradually decays and an effective chemical interaction changes sign [3,5]. In the high-Cr alloys, the effective interactions exhibit a phase-separation character, which in turn affects the concentration dependence of the mixing enthalpy. As a result, one sees a change in the curvature of the mixing enthalpy which indicates a tendency towards spinodal decomposition in the system.

In addition to thermodynamic characteristics, first-principles methods were quite successful in calculations of the mechanical properties of Fe-Cr alloys. In Ref. [11] the exact muffin-tin orbitals (EMTO) method was used to study the elastic properties of pure iron and Fe-Cr alloy with 10 at % Cr. In this work the authors obtained the temperature dependences of the bulk modulus B , the elastic coefficients C' and C_{44} , and the coefficient of anisotropy using electronic and magnetic contributions, as well as considering the thermal expansion of the lattice [11]. The authors showed that the degree of magnetic order in both pure iron and Fe₉₀Cr₁₀ alloy mainly determined a sharp change in the elastic anisotropy at finite temperatures. The lattice expansion effect in these materials was secondary but still very important for the quantitative analysis. In Ref. [12] the authors investigated the elastic properties of bcc Fe_{1-c}Cr_c alloys ($0 \leq c \leq 1$) in the ferromagnetic and paramagnetic states. The concentration dependences of the elastic constants C_{11} and C_{44} , and the elastic moduli B and E were calculated [12]. Comparison with experimental data showed that the theoretical approach was fairly accurate. The authors observed the nonmonotonic relation of the elastic constants on the composition and argued that it should have a significant effect on the micromechanical properties of ferritic stainless steels.

Besides the elastic properties and the mixing enthalpy, the lattice parameter of Fe-Cr alloys also shows an anomalous composition dependence at about 5 at % Cr [13]. Using the EMTO calculations the authors suggested that the observed anomalies were related to the electronic topological transition in these alloys. The concentration dependences of the elastic coefficients C_{11} , C_{12} , and C_{44} , the elastic moduli B , G , and E , the Poisson coefficient, and the Debye temperature were also calculated [13]. Some of these characteristics exhibited anomalous behavior at Cr concentration close to 5 at %. Theoretical data on the Poisson coefficient and elastic moduli B and G presented in Ref. [13] were in good agreement with experimental data [14], although theoretical calculations overestimate the Young's modulus E .

In Ref. [15] the authors studied the phase stability of binary fcc and bcc Fe-Cr, Fe-Ni, and Cr-Ni alloys and ternary Fe-Cr-Ni alloys using a combination of DFT calculations, cluster expansion, and magnetic cluster expansion. Using the database of 248 fcc and 246 bcc configurations, the authors evaluated the stability of the fcc and bcc Fe-Cr-Ni ternary alloys. Theoretical analysis of multicomponent alloying of Ni, Mn, and Mo on the phase stability of bcc Fe-Cr solid

solutions was performed in Ref. [16]. Li *et al.* [17] used the EMTO method in combination with the coherent potential approximation to study the effect of alloying with V, Cr, Mn, and W on the mechanical properties of Fe₉₁Cr₉ solid solution. The authors showed that W, Cr, and V increased the elastic constants C_{11} and C_{12} and the Young's modulus of the alloys. Manganese, on the other hand, reduced the elastic constants C_{11} and C_{12} [17].

Thus theoretical study of the effects of alloying on the thermodynamic and mechanical properties of the Fe-Cr-based alloys is a highly relevant task. Still, despite the huge interest in the first-principles studies of this system, there is limited knowledge on the effects of the multicomponent alloying. In this work we perform first-principles calculations of the lattice parameters, mixing enthalpies, and magnetic and elastic properties of bcc Fe-Cr-based alloys containing up to 20 wt % Ni, as well as with small concentrations of other alloying elements, Mo, Al, W, V, and Nb. We present and discuss properties of bcc solid solutions at zero temperature, even though in some cases the alloying with considered concentrations of elements in practice may lead to phase transitions at finite temperature. However, broadening the concentration interval for modeling of bcc solid solution allows us to clearly identify trends in the behavior of the calculated properties.

II. DETAILS OF THE CALCULATIONS

Electronic-structure and total-energy calculations were carried out at temperature $T = 0$ K in the framework of the exact muffin-tin orbitals method combined with the coherent potential approximation (CPA) for modeling of substitutional disorder [18,19]. The numerical efficiency of the method allowed us to carry out high-throughput simulations, while the reliability of the method in predicting thermodynamic properties and elastic moduli of bcc Fe-Cr alloys has been demonstrated in literature [2–6,11,12]. We used a computational setup similar to that described in Ref. [16]. The full charge density (FCD) [20] was represented by a single-center expansion of the electron wave functions in terms of spherical harmonics with orbital moments $J_{\text{FCD}}^{\text{max}}$ up to 8. Self-consistent electron densities were obtained within the local-spin-density approximation (LSDA) [21], while the total energies were calculated in the generalized gradient approximation (GGA) [22]. The reliability of the treatment of the exchange and correlation effects employed in the present work was demonstrated earlier and reviewed in Ref. [23]. Integration in the reciprocal space was performed over a grid of $37 \times 37 \times 37$ k points. The energy integration was carried out in the complex plane using a semielliptic contour comprising 24 energy points. Calculations were performed for a basis set including valence *spdf* orbitals. We have considered collinear alignment of magnetic moments. Ferromagnetic configurations with local magnetic moment values equal to $2 \mu_B$ were set as initial guesses. Both values and directions of the magnetic moments were calculated self-consistently without any constrain. The elastic constants were calculated from the strain dependences of total energies as described in Ref. [18]. The polycrystalline elastic moduli were obtained using the averaging of the theoretical single crystals elastic constants using the Hill (H) procedure [18]. To perform calculations efficiently, we

developed a PYTHON 3-based workflow (see Supplemental Material [24]).

We note that the EMTO-CPA method treats the completely disordered alloys without any short-range order. In addition, the method does not allow one to include the effect of the local lattice relaxations present in random alloys. To evaluate the importance of the latter in the studied systems, we carried out selected calculations employing supercells, constructed as the special quasirandom structures (SQS) [23,25] and projector augmented wave (PAW) [26] method. Unlike the EMTO-CPA technique, the SQS-PAW calculations allow for the local atomic relaxations and provide us with an estimation of their effect on the properties calculated in this work. We have performed PAW-SQS calculations for selected bcc Fe-Cr, Fe-Cr-Ni, and Fe-Cr-Ni-Al alloys using the VASP software [27,28]. To investigate the influence of the supercell size, the bcc alloys were modeled by SQS supercells of two sizes: $3 \times 3 \times 3$ (54 atoms) and $4 \times 4 \times 4$ (128 atoms). Integration over the Brillouin zone was performed on a $4 \times 4 \times 4$ and $3 \times 3 \times 3$ k -point grid for supercells containing 54 and 128 atoms, respectively. Sampling for Brillouin zone was carried out using the first-order Methfessel-Paxton smearing method and the width of smearing was set to 0.2 eV [29]. The exchange-correlation effects were treated using the GGA [22]. We used the recommended PAW potentials, and the cutoff energy of plane waves was set to 520 eV. As in the EMTO-CPA calculations, we treated the magnetic moments as collinear, setting the initial configuration as ferromagnetic. Initial values of the local magnetic moments were set equal to $3\mu_B$ and then their values and directions evaluated self-consistently.

For PAW-SQS simulations the elastic constants of the cubic crystal were calculated via the stress-strain relations. To do this we applied a non-volume-preserving strain to the cubic cell structure, given in the form [30]

$$\delta\epsilon = \begin{pmatrix} e & \frac{e}{2} & 0 \\ \frac{e}{2} & 0 & 0 \\ 0 & 0 & 0 \end{pmatrix}, \quad (1)$$

where $\delta\epsilon$ denotes the strain matrix and e is the relative strain. The elastic constants of a cubic crystal were defined as follows:

$$\sigma_{xx} = c_{11}e, \quad \sigma_{yy} = c_{12}e, \quad \sigma_{xy} = c_{44}e, \quad (2)$$

where σ_{xx} , σ_{yy} , σ_{xy} denote the components of the stress tensor calculated within the PAW-SQS method, and c_{11} , c_{12} , c_{44} denote the elastic constants of the cubic crystal.

In this work we applied the values of the relative strain e in the range $[-4\%, +4\%]$ with a step of 1%. The elastic constants were defined as coefficients of a linear regression via minimization of the mean square error. In order to estimate nonlinear effects in a given distortion interval we considered different numbers of distortions: -1% and 1% ; -1% , 0% ; and 1% ; as well as all other distortions in the range $[-4\%, +4\%]$ (see Fig. 1). The mixing enthalpies and elastic constants of the Fe-Cr, Fe-Cr-Ni, and Fe-Cr-Ni-Al alloys were calculated for the SQS structural models considering to two cases—fully relaxed and ideal nonrelaxed bcc positions of the atoms in the supercell.

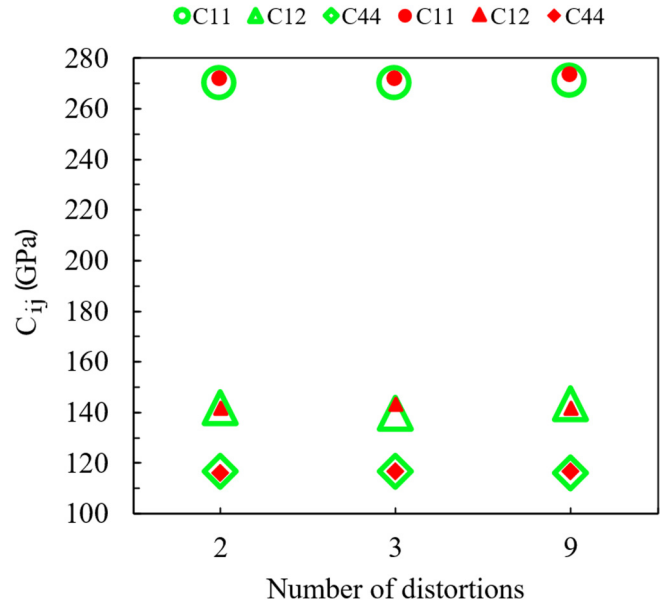


FIG. 1. Effect of local lattice relaxations on elastic constants of Fe-12%Cr. Green symbols correspond to nonrelaxed calculations, while red symbols represent relaxed structures. Here the SQS consists of 54 atoms.

To determine the equilibrium lattice parameters, total energy in the ground state, bulk moduli, and their pressure derivatives, we calculated the alloys total energies as a function of alloy volumes and fitted the results using the Birch-Murnaghan equation of state [31]. Zhang *et al.* showed [32] that the choice of the fitting interval affected the calculated bulk modulus of bcc Fe due to the presence of a magnetic transition that occurred when volume changed. We have also identified this transition in several alloys studied in this work. However, the sharp magnetic transitions occur only at expanded volumes, as seen, for example, in Fig. S2 of the Supplemental Material [24]. (If the transition is smeared out, it has much smaller influence on the calculated parameters of the equation of state.) Consequently, we avoid the problem by including in the fitting volumes that do not substantially exceed the expected equilibrium volume.

III. ANALYSIS OF APPROXIMATIONS UNDERLYING SIMULATIONS OF THERMODYNAMIC AND ELASTIC PROPERTIES OF MULTICOMPONENT bcc Fe-Cr-BASED ALLOYS

A. Local lattice relaxations

Let us first consider the effect of the local lattice relaxations on equilibrium volumes V_0 , the bulk moduli B , their derivatives B' , and mixing enthalpies ΔH of the three bcc systems: Fe-(12 wt %)Cr, Fe-(10 wt %)Cr-(2 wt %)Ni and Fe-Cr-Ni-Al. All alloys were calculated for the SQS of two different sizes and with varying arrangements of atoms. The results are listed in Table I, as well as the exact weight concentrations in the model structures.

For Fe-12%Cr alloy the mixing enthalpies ΔH , calculated with and without atomic relaxations, differ by 1 meV, which is comparable to the numerical accuracy of the calculated total

TABLE I. Total energies, bulk moduli B , their pressure derivatives B' , equilibrium volume V_0 , and mixing enthalpies ΔH of bcc Fe-Cr, Fe-Cr-Ni, and Fe-Cr-Ni-Al systems calculated at $T = 0$ K (see Supplemental Material [24] for conversion between units).

No.	Alloy composition (wt %)/model	Total energy eV/atom	B GPa	B'	V_0 Å ³ /atom	ΔH eV/atom
1	Fe-12.1%Cr (54 atoms) nonrelaxed	-8.392	181	5.1	11.46	0.010
2	Fe-12.1%Cr (54 atoms) relaxed	-8.393	181	5.1	11.46	0.009
3	Fe-11.7%Cr (128 atoms, No. 1) relaxed	-8.387	178	5.2	11.47	0.008
4	Fe-12.4%Cr (128 atoms, No. 2) relaxed	-8.394	179	5.2	11.46	0.011
5	Fe-10.4%Cr-1.9%Ni (54 atoms) relaxed	-8.314	175	5.3	11.47	0.012
6	Fe-10.2%Cr-1.6%Ni (128 atoms) relaxed	-8.321	175	5.3	11.47	0.011
7	Fe-8.9%Cr-10.0%Ni-2.8%Al (54 atoms) nonrelaxed	-7.862	162	5.0	11.59	-0.012
8	Fe-8.9%Cr-10.0%Ni-2.8%Al (54 atoms), relaxed	-7.871	160	5.2	11.60	-0.022
9	Fe-9.7%Cr-10.9%Ni-2.3%Al (128 atoms) nonrelaxed	-7.877	167	4.9	11.58	-0.003
10	Fe-9.7%Cr-10.9%Ni-2.3%Al (128 atoms) relaxed	-7.886	166	4.9	11.58	-0.012

energies. In addition, the lattice relaxations do not have significant impact on V_0 , B , and B' . In fact, the size of the SQS, as well as the difference in distributions of atoms within the SQS of the same size (shown in rows 3 and 4 of Table I), have somewhat stronger impact on the calculated properties: the difference in the mixing enthalpy increases to 3 meV, which is still well within the accuracy of interest for the present work. Moreover, the bulk modulus for the two models differ by less than 2%. In the case of the Fe-10%Cr-2%Ni system, two different sizes of the SQS give the difference in ΔH of ~ 1 meV, and the changes in elastic properties and equilibrium volume are also insignificant.

The size of an aluminum atom is larger than that of iron, chromium, and nickel. Therefore the effect of the lattice relaxations is expected to be stronger in Fe-Cr-Ni-Al alloys than in the Fe-Cr and Fe-Cr-Ni alloys. Indeed, the difference in the total energies and mixing enthalpies between the relaxed and unrelaxed Fe-Cr-Ni-Al alloys increases, but it remains within 10 meV, which is comparable to the experimental accuracy of measuring the enthalpy. The difference in equilibrium volumes and bulk moduli remains negligible.

In Fig. 1 we show the effect of the local lattice relaxations on the elastic constants of the Fe-12%Cr system. Here the elastic constants are calculated for both relaxed and nonrelaxed structures and are shown as a function of number of distortions in the strain range $[-4\%, +4\%]$. It turns out that the elastic constants vary slightly as the number of distortions changes, even when the strain interval increases up to $\pm 4\%$. Most importantly, according to Fig. 1 the local lattice relaxations have very little effect on the elastic constants of the bcc Fe-12%Cr. A similar conclusion can be drawn for systems containing Ni and Al, the elastic constants of which are affected by less than 10 GPa by the local lattice relaxations, see Table II.

Note that a promising technique to evaluate the elastic interaction correction to the total energy of a defect in a material has been described by Varvenne *et al.* [33] and by

Ma and Dudarev [34]. However, so far it has been applied for the cases of point defects or their clusters in elemental materials. Generalization of the technique for the concentrated substitutional alloys considered in our study appears as a subject of an independent study. The supercell calculations carried out above for Fe-Cr, Fe-Cr-Ni, and Fe-Cr-Ni-Al alloys indicate that the neglect of the local lattice relaxations in our EMTO-CPA calculations is a reasonable approximation for the purposes of this work.

B. Electrostatic contribution to one-electron potential and energy of substitutional alloys within CPA

There are some additional approximations in the EMTO-CPA method which require further justification in applications. In particular, the electrostatic contribution to the one-electron potential and energy of a substitutional alloy cannot be consistently calculated within the single-site approximation upon which the CPA is based [23]. The screened impurity model (SIM) was suggested in [35] to address this problem and subsequently refined in several works, with the most advanced form presented by Ruban *et al.* in [36,37]. In the framework of the SIM, the on-site potential v^p can be

TABLE II. Elastic constants of Fe-Cr-Ni-Al alloys.

Alloy composition (wt %)/model	C_{11} GPa	C_{12} GPa	C_{44} GPa	C' GPa
Fe-8.9%Cr-10.0%Ni-2.8%Al (54 atoms) nonrelaxed	218	141	117	38
Fe-8.9%Cr-10.0%Ni-2.8%Al (54 atoms) relaxed	224	140	120	42
Fe-9.7%Cr-10.9%Ni-2.3%Al (128 atoms) nonrelaxed	221	139	116	41
Fe-9.7%Cr-10.9%Ni-2.3%Al (128 atoms) relaxed	229	141	118	44

corrected with term Δv^p :

$$\tilde{v}^p = v^p + \Delta v^p = v^p - \alpha_p^{(1)} \frac{q_p}{S}, \quad (3)$$

where $\alpha_p^{(1)}$ denotes the local screening constant, $\alpha_p^{(1)} \leq 1$. The necessary shift of the total energy is determined as

$$E^{CPA} = \bar{E} - \sum_p c_p \alpha_p^{(1)} \beta_p \frac{q_p^2}{2S}, \quad (4)$$

where \bar{E} is determined as a configurationally averaged energy of contributions calculated for each alloy component.

It was demonstrated that universal values of the parameters $\alpha_p^{(1)} \sim 0.6$ and $\beta_p \sim 1$ provided very good agreement between charges and energies calculated using the CPA and a supercell approach [38]. Moreover, the agreement may be further improved using the procedure proposed in [36,37]. We have followed it in the present work employing the locally self-consistent Green's function (LSGF) [39,40] method implemented within the exact muffin-tin orbital technique (ELSGF) [41]. The ELSGF method has allowed us to calculate exactly the electrostatic contribution to the one-electron potential and total energy of a substitutional alloy simulated by means of a large SQS. Because we have used exactly the same computational parameters in ELSGF calculations for selected alloys as in the EMTO-CPA calculations (see Sec. II), the comparison between the two methods might improve the choice of the SIM parameters $\alpha_p^{(1)}$ and β_p . It has turned out that we could use the universal value of $\beta_p = 1.1$. The set of parameters $\alpha_p^{(1)}$ employed in the present study is summarized in Table S1 (see Supplemental Material [24]). We note that for some Fe-Cr-Ni and Fe-Cr-Ni-Al alloys we have not succeeded in determining the $\alpha_p^{(1)}$ parameters self-consistently. However, the parameters given in Table S1 of the Supplemental Material [24] still provide a quite accurate description of the charge transfer and the total energies of the alloys.

C. Treatment of core electrons in the EMTO method

The EMTO method is an all-electron method, but the core and valence electrons are treated differently [18]. While the latter one solves the Kohn-Sham problem for the crystal potential, the former are recalculated at each iteration of the charge self-consistency loop considering the atomic sphere approximation for the alloy crystal potential (the so-called soft-core calculations). However, the charge density of the core electrons may be frozen to that obtained in atomic calculations for individual alloy components in the so-called frozen-core approximation. While the soft-core calculations should provide self-consistent all-electron results, it has been demonstrated earlier that in Fe-based alloys the frozen-core approximation could lead to somewhat better agreement with experiment due to better agreement between the calculated lattice parameters and their room-temperature experimental values [42].

In Fig. 2 ground-state properties such as lattice parameters, mixing enthalpies, bulk moduli, single-crystal elastic constants, Young's moduli, shear moduli, and G/B ratios obtained for bcc Fe-Cr alloys using the frozen-core approximation and the soft-core calculations are compared with our PAW-SQS results and with the experimental data. The figure shows the

reliability of using the frozen-core approximation. Indeed, the Fe-Cr system exhibits an anomalous stability of the ferromagnetic disordered alloys at a low chromium concentration, which is reflected in the calculated negative sign of the mixing enthalpy at Cr concentrations below 10 wt %. The lattice parameters exhibit slightly nonlinear dependence as a function of Cr concentration. The soft-core calculations underestimate the values of the lattice parameter, while the frozen-core approximation overestimates them. However, the latter leads to the lattice parameters of the alloys, which are somewhat closer to the experimental data measured at room temperature. In addition, values of the elastic constant C_{11} , Young's modulus, and bulk modulus calculated for pure bcc Fe and low-Cr alloys in the frozen-core approximation agree better with experiment, while the soft-core calculations more accurately describe the shear constant C_{44} . All in all, the frozen-core approximation appears to give somewhat better agreement with the experiment, most likely due to better agreement between the calculated and experimental (room-temperature) lattice parameter. Therefore, in Sec. IV we present the EMTO-CPA results obtained within the frozen-core approximation. Note that we carried out the soft-core calculations for selected systems considered in our study and did not detect any qualitative differences in the influence of the multicomponent alloying on the studied materials parameters due to the use of the frozen-core approximation.

IV. RESULTS AND DISCUSSION

A. Lattice parameters

First we determine the equilibrium lattice parameters of ferromagnetic bcc Fe-Cr(0–20 wt %)-Ni(5–20 wt %)-X alloys with $X = \text{Nb, V, W, Mo, Al}$. Their values are shown in Fig. 3 as a function of chromium concentration at fixed concentrations of Ni and X elements. Note that in this figure and in the following, the compositions with zero chromium content $x_{\text{Cr}} = 0$ correspond to pure bcc Fe in case of Fe-Cr alloys and to binary Fe-Ni or Fe-X alloys otherwise.

For the binary Fe-Cr alloys in the range of Cr concentration 0–20 wt %, the lattice parameter a shows positive deviation from the Vegard law. For multicomponent alloys containing 1 wt % Nb, V, W, or Mo, the lattice parameter curves lie above the Fe-Cr one; however, the concentration behavior of the lattice parameters is weakly affected by the alloying with these elements. The lattice parameters of the three-component Fe-Cr-Ni alloys decrease with increasing Ni concentration, though for $x_{\text{Cr}} < 5\%$ they are higher than in the binary Fe-Cr alloys. Note that the higher the Ni concentration, the more pronounced the decrease of a . For aluminum-containing alloys Fe-Cr(0%–20%)-Al(2.5%–5.0%) the lattice parameters are larger compared to other ternary alloys and they slightly decrease with increasing x_{Cr} . In four-component alloys with 5 wt % Ni, all the lattice parameter curves go up, and the maximum values correspond to alloys with 5 wt % Al. With increasing nickel content, all the curves go down proportionally to the nickel content.

Summarizing our calculations of the lattice parameters, we see that the alloying elements Nb, V, W, Mo, or Al increase the lattice parameter, which can be explained by their larger

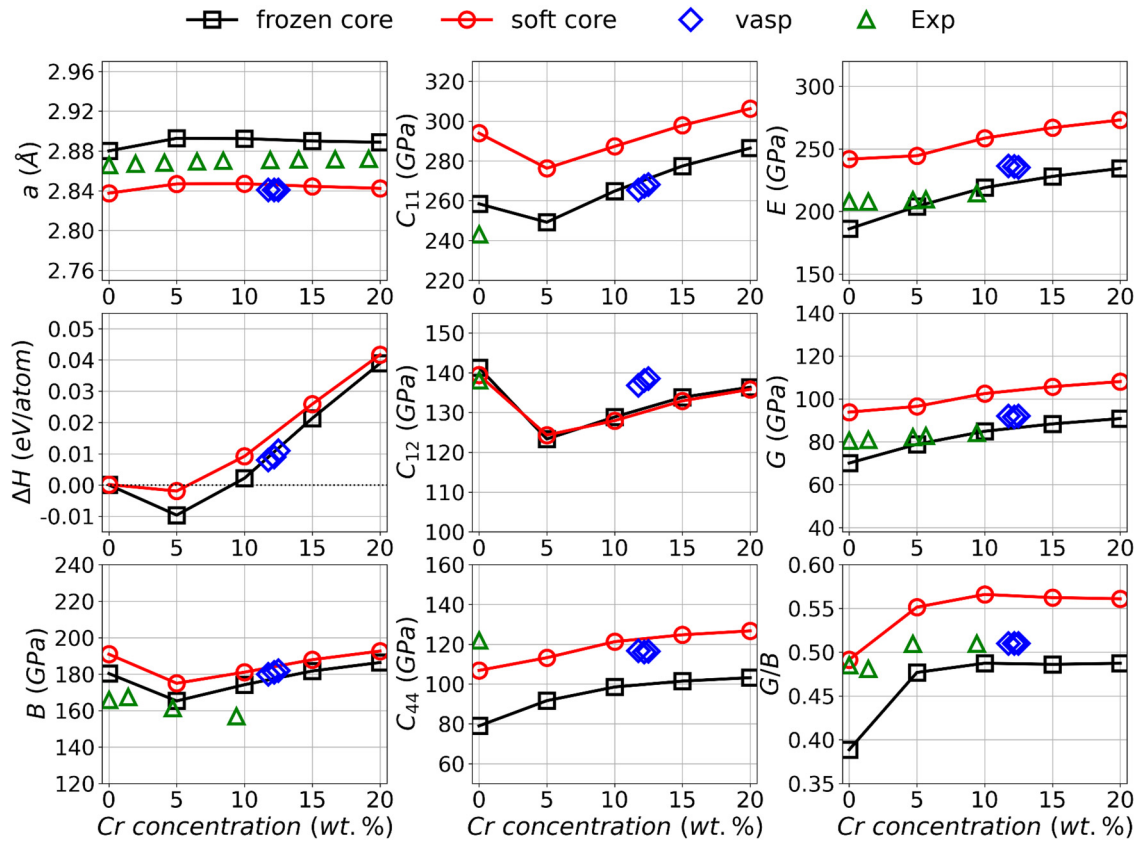


FIG. 2. Lattice parameters a , mixing enthalpies ΔH , bulk moduli B , single-crystal elastic constants C_{11} , C_{12} , and C_{44} , Young’s moduli E , shear moduli G , and G/B ratios obtained for bcc Fe-Cr alloys using the EMTO-CPA method in the frozen-core approximation (black squares) and soft-core calculations (red circles). Results of our VASP calculations (blue diamonds) and experimental results from [14,43–45] (green triangles) are shown for comparison.

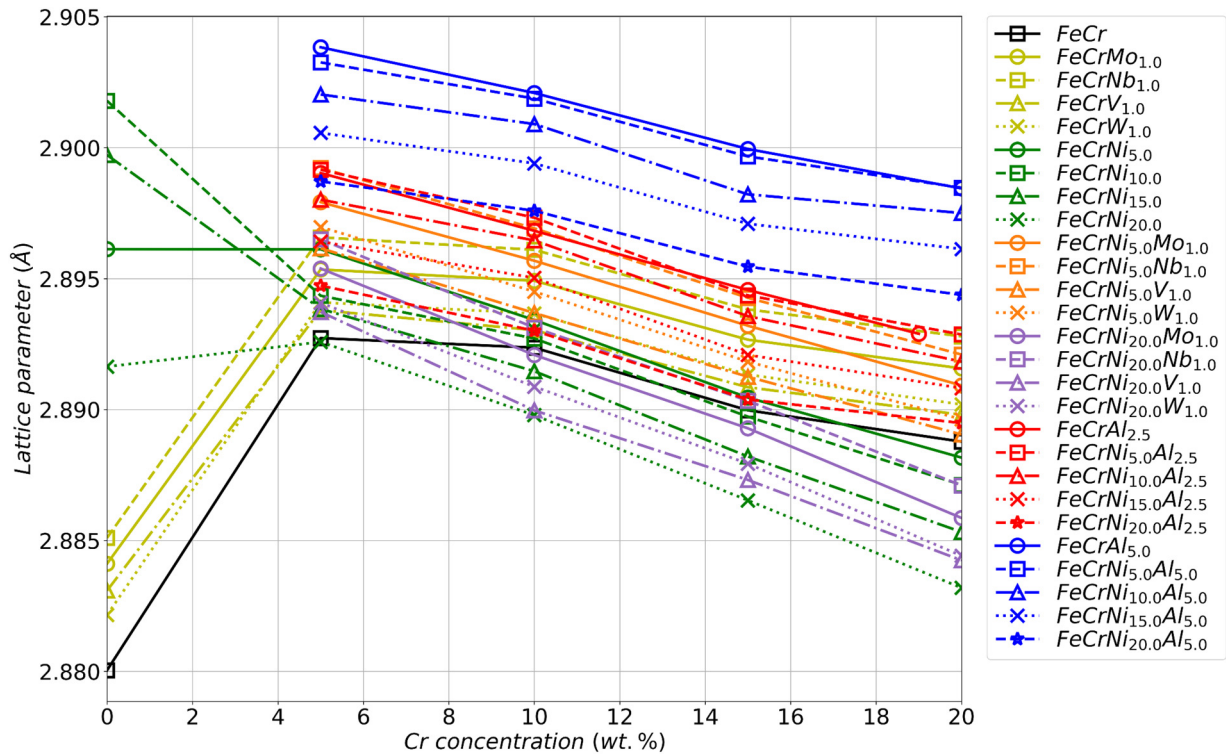


FIG. 3. Effect of multicomponent alloying on lattice parameters of bcc Fe-Cr-based alloys.

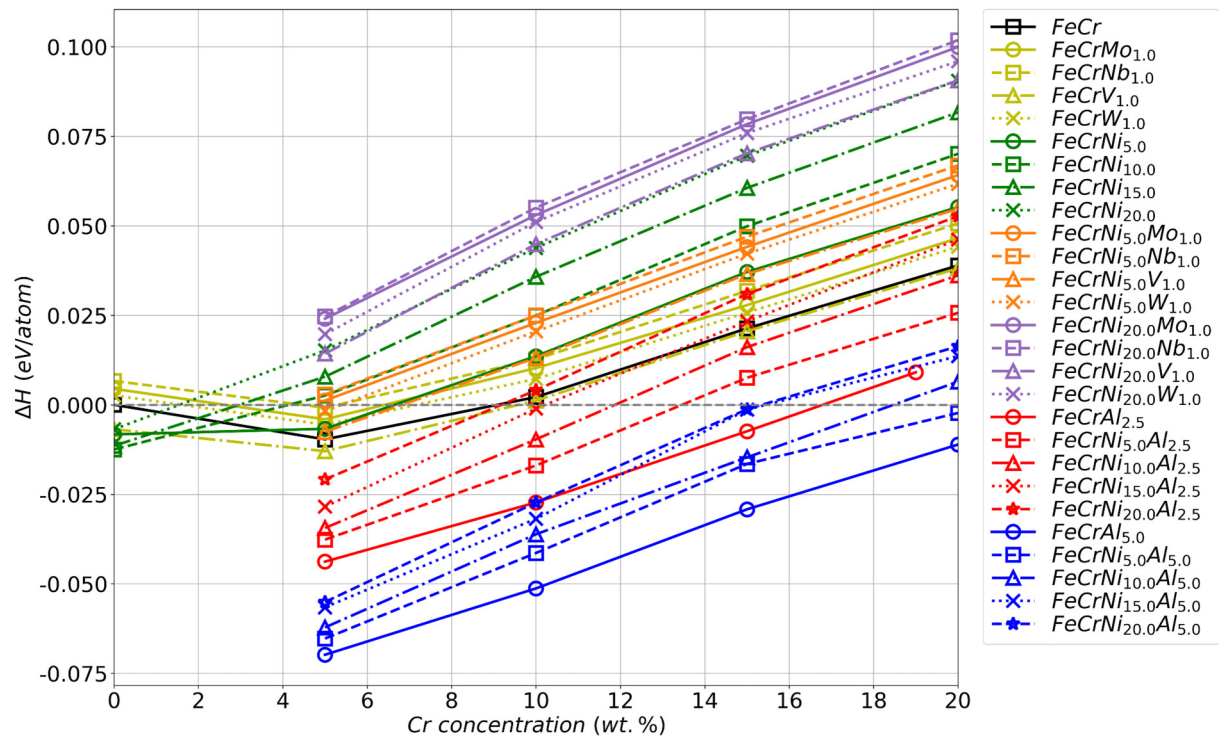


FIG. 4. Effect of multicomponent alloying on mixing enthalpy ΔH of bcc Fe-Cr-based alloys.

atomic radius. Nickel and chromium in alloys with $x_{\text{Ni,Cr}} > 5$ wt % reduce the lattice parameter. In four-component alloys containing nickel, which reduces the lattice parameter, the impact of aluminum is stronger. Therefore the increase of the lattice parameters of Fe-Cr(0–20 wt %)-Ni(5–20 wt %)-Al (5.0 wt %) alloys is the strongest among all the studied systems.

B. Mixing enthalpy

Figure 4 shows the calculated mixing enthalpies ΔH of the studied alloys. The mixing enthalpies were calculated with respect to pure elements: ferromagnetic (FM) bcc Fe, bcc Cr in the nonmagnetic (NM) state, FM fcc Ni, NM fcc Al, bcc Mo, V, W.

The mixing enthalpy of the binary Fe-Cr alloy has a minimum at ~ 5 wt % Cr, and the alloys are predicted to be stable up to ~ 10 wt % Cr at zero temperature. With addition of 1 wt % Nb, V, W, Mo the minimum of the mixing enthalpy remains at ~ 5 wt % Cr. Vanadium enhances the stability of low-chromium alloys and broadens the stability region. On the contrary, W, Mo, and Nb narrow it. ΔH plots of vanadium-containing alloys are lower compared to Fe-Cr alloys for the entire studied interval of Cr concentrations (0–20 wt % Cr). Alloying with Ni increases the stability of the low-chromium Fe-Cr alloys (1–3 wt % Cr). However, Ni narrows the stability interval of these alloys with respect to Cr concentration, and the higher the nickel content the stronger the effect. Thus when the concentration of Ni reaches 20 wt % the ternary Fe-Cr-Ni alloys are only stable up to $x_{\text{Cr}} \sim 1.5\%$.

The additions of 1 wt % Nb, W, or Mo to ternary Fe-Cr(0–20 wt %)-Ni (5–20 wt %) alloys lead to a further decrease of their stability, and Nb provides the largest destabilizing effect in four-component alloys at constant Ni concentrations. Vanadium has a very weak stabilizing effect on alloys with 5–15 wt % nickel and a weak destabilizing effect on alloys with 20 wt % nickel. The mixing enthalpy of ternary Fe-Cr-Al alloys with 2.5 wt % Al is well below the enthalpy calculated for the binary Fe-Cr alloys. Interestingly, the interval of stability in terms of Cr concentration increases up to 17 wt % Cr. When Al content reaches 5.0 wt % the ΔH curve goes even lower and is negative for all studied Cr concentrations. Moreover, the alloys containing 5.0 wt % Al have the most negative mixing energy. Nickel has a destabilizing effect in aluminum-containing alloys: ΔH of all nickel and aluminum-containing alloys are higher compared to nickel-free aluminum-containing alloys. For example, ΔH of Fe-Cr(0%–20%)-Ni(5%)-Al(2.5%) is higher compared to Fe-Cr(0%–20%)-Al(2.5%). The higher the nickel content the stronger its destabilizing effect.

Summarizing our calculations of the mixing enthalpy of multicomponent Fe-Cr-based bcc alloys, we see that Ni destabilizes the alloys, and the effect is enhanced by the addition of 1 wt % Nb, W, or Mo. However, the addition of aluminum to Fe-Cr binary or Fe-Cr-Ni ternary alloys increases their stability with respect to decomposition into pure alloy components.

C. Magnetic moments

Figure 5 shows the local (on-site) magnetic moments at Fe atoms (a), the total (net) magnetic moments of Fe-Cr-X alloys (b) and the local moments of Cr (c). The local magnetic

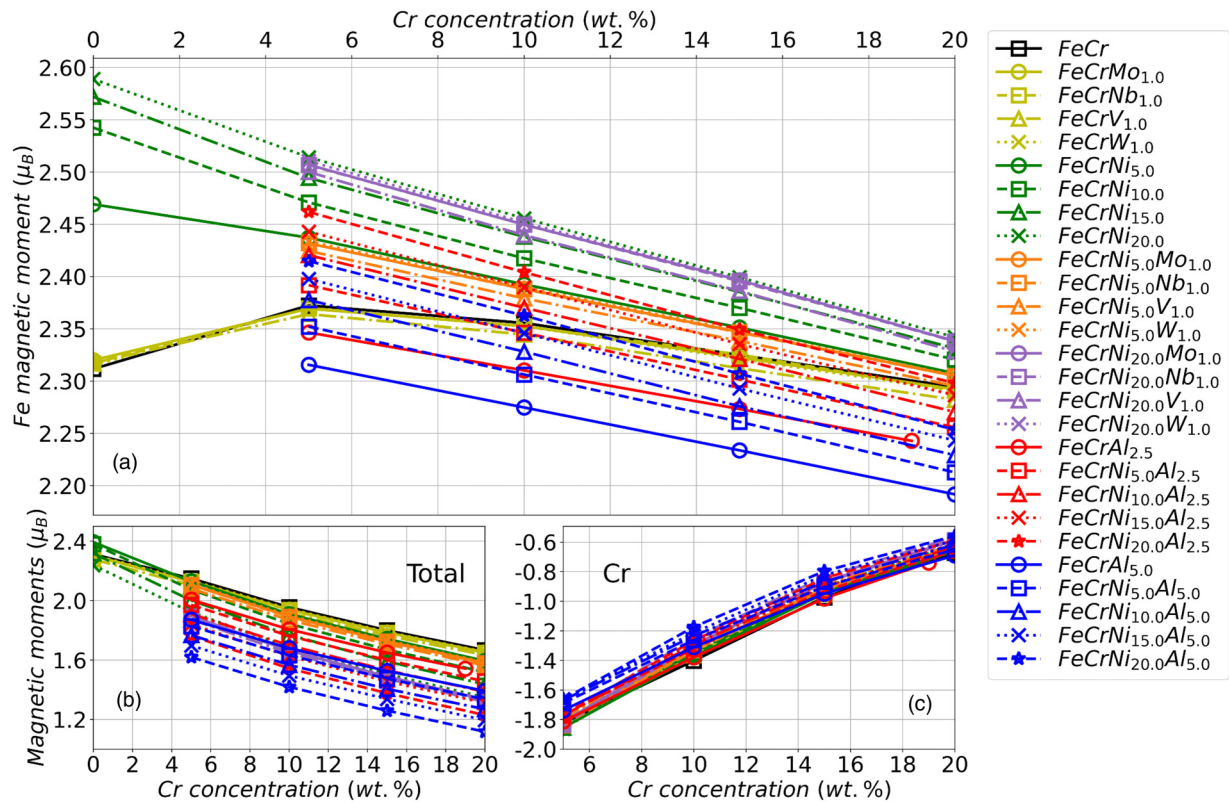


FIG. 5. Effect of multicomponent alloying on magnetic moments of bcc Fe-Cr-based alloys.

moments of Ni, as well as moments induced at Nb, V, W, Mo, and Al atoms are shown in Figs. S3 and S4 in Supplemental Material [24].

The total magnetic moment (MM) of all the studied alloys decreases with increasing chromium content [see Fig. 5(b)]. For the binary Fe-Cr alloys, the total MM are higher compared to other studied alloys, except for Fe-Ni alloys with low Ni concentration. This is in agreement with a general dependence of the net magnetization in alloys based on 3d transition metals on the electron concentration, known as the Slater-Pauling curve. The total MM of Fe-Cr(0–20 wt %)-X(1 wt %) alloys (where $X = \text{Nb, V, W, Mo}$) becomes smaller, and the decrease of the net magnetization due to the alloying effect is stronger in the following order of the considered alloying elements: W, Nb, Mo, V. The effect comes from the antiferromagnetic alignments of local moments induced at these impurities, which have relatively large magnitudes (Fig. S4 in the Supplemental Material [24]). Addition of nickel above $x_{\text{Ni}} \sim 10\text{wt \%}$ to alloys with $x_{\text{Cr}} > 5\text{wt \%}$ significantly decreases the values of the MM. Though Ni and Fe local moments are aligned ferromagnetically, the values of the local moment at Ni decrease rapidly with increasing Cr concentration according to our analysis (see Fig. S3 in Supplemental Material [24]). Aluminum significantly reduces the net magnetization of the alloys. Here the effect mostly comes from the influence of Al on magnitudes of the local moments of other transition metals in the alloy: they decrease with increasing Al concentration [Figs. 5(a) and 5(c), Fig. S3 in Supplemental Material [24]]. The induced magnetic moment on Al is aligned antiparallel to the net magnetization,

but it is quite small. The maximum decrease of the MM is observed in alloys containing both Ni and Al.

Recent studies [3–6] showed that the values of the pair magnetic exchange interactions between Cr atoms in Fe-Cr alloys are negative, and therefore the presence of a pair of Cr atoms as the nearest neighbors causes magnetic frustration, leading to a gradual quenching of the magnetic moment on chromium atoms with increasing Cr concentration [3]. In the present study of the multicomponent alloys, we observe similar behavior of the local magnetic moment at Cr. Moreover, the impact of Cr concentration on the decrease of the net MM is much stronger than the impact of any other alloying element. The change of Cr magnetic moment versus its concentration almost completely reproduces the concentration behavior of the total magnetic moment, except for highly diluted alloys and aluminum-containing alloys (Fe-Cr-Al_{5.0}) with chromium concentration of $\sim 15\text{--}20\text{ wt \%}$.

Let us next consider in more detail the magnetic moments of the Fe atoms [Fig. 5(a)]. When nickel is added, the Fe MM increases: the more Ni is added, the higher the Fe moment (at a fixed Cr concentration). Alloys with aluminum show the opposite trend, that is, the higher the Al content, the lower the Fe moment. Thus Fe moments in nickel-containing alloys Fe-Cr(0%–20%)-Ni(20%) are higher than for all other alloys at the fixed chromium concentration considered in this study. On the contrary, in the aluminum-containing alloys Fe-Cr(0–20 wt %)-Al(5 wt %) the Fe moment is the smallest. Comparing this observation with the trend observed for the mixing enthalpy ΔH vs x_{Cr} (Fig. 4), we see an interesting correlation between the two

properties: the elements that decrease magnetic moment on Fe atoms increase the stability of the respective alloys and vice versa.

The observed correlation may not be accidental. Indeed, it is well established in the literature that the antiferromagnetic coupling between Fe-Cr and Cr-Cr magnetic moments leads to frustrating effects due to conflicting exchange interactions, contributing to the destabilization of the system with higher Cr concentration. A detailed analysis of chemical and magnetic interactions in Fe-Cr alloys carried out in Ref. [6] in terms of the Hamiltonian combining both chemical and magnetic degrees of freedom showed that at the ambient pressure, the effective pair interactions at the first coordination shell have strong concentration dependence determined mostly by the Fe-Cr magnetic exchange interactions. On the other hand, magnetic exchange interactions for Fe-Fe and Cr-Cr nearest neighbors almost compensated each other. It was also shown that the balance was sensitive to magnitudes of the magnetic moments: when Cr local moments were reduced, ferromagnetic Fe-Fe exchange interactions started to dominate. They contributed to increasing tendency towards clustering in the alloy Hamiltonian, and the larger the Fe moments, the stronger the contribution. Of course, the situation becomes more complicated in multicomponent alloys, as was demonstrated in Ref. [16]. Considering two systems, including $\text{Fe}_{100-c-05}\text{Cr}_c\text{Ni}_{05}$ alloy, which is of interest for our study, the author of Ref. [16] showed that the stabilizing effect of Fe-Cr magnetic exchange interactions was indeed compensated by other competing exchange interactions, increasing the importance of ferromagnetic Fe-Fe exchange interactions in the alloy Hamiltonian. Of course, the effect may be system dependent, and the origin of the observed correlation between amplitude of Fe magnetic moments and mixing enthalpies of the multicomponent alloys requires a detailed study that is beyond the subject matter of the present work.

The destabilization of alloys with increasing Cr and Ni concentrations is also reflected in calculations of the electronic density of states (DOS), shown in Fig. 6. In the low-chromium binary alloy $\text{Fe}_{95}\text{Cr}_{05}$ the Fermi level is located in the pseudogap of the minority-spin channel. With increasing chromium concentration and due to a decrease in the magnetic moment, the minority-spin states shift to lower energies. Therefore the Fermi level crosses the ascending branch of the DOS peak, which makes the alloys energetically less favorable. As a result, the ΔH increases with an increase in the chromium concentration. In aluminum-containing ternary alloys (shown by the example of $\text{Fe}_{80}\text{Cr}_{15}\text{Al}_{05}$), due to a decrease in the electron density and p - d hybridization, the peak again is at the minimum of the pseudogap. On other hand, in the nickel-containing alloys the Fermi level crosses a peak formed by the e_g states of nickel. This is a destabilizing factor indicating that the solid solution becomes less stable with respect to decomposition into pure elements.

D. Single-crystal elastic constants

The elastic response of the studied alloys to uniaxial strain $(100)(100)$ can be characterized by the elastic constant C_{11} . They are plotted in Fig. 7. Additions of 1 wt %

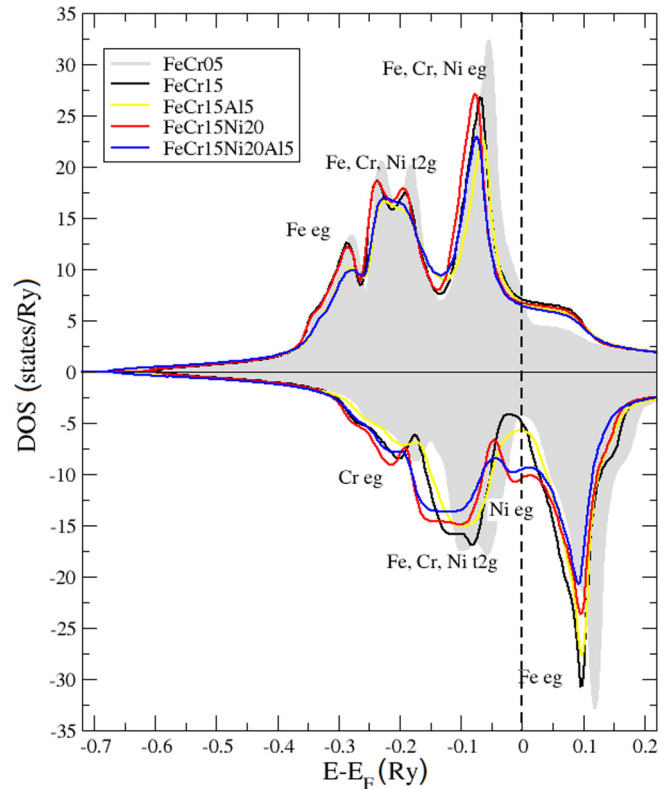


FIG. 6. Effect of alloying with Ni and Al on the electronic density of states (DOS) of bcc Fe-Cr-based alloys.

Nb, V, W, or Mo do not modify qualitatively the dependence of the elastic constants on Cr concentration, though one sees that they increase slightly at Cr concentrations above 5 wt %. Concentration dependence of the elastic constant C_{11} in binary Fe-Ni alloys appears to be nonmonotonous. An addition of 5 wt % Ni decreases C_{11} , but with increasing Cr concentration the influence of the latter dominates and C_{11} increases. Increasing Ni concentration decreases C_{11} further: one observes a minimum at the corresponding curve at ~ 10 wt % Cr. All the curves for alloys containing Ni are below the C_{11} curve for the binary Fe-Cr alloy, and the higher the nickel content, the lower the elastic constant. The curves of Al-containing ternary alloys Fe-Cr(0–20 wt %)-Al(2.5–5 wt %) lie between the curves of the binary Fe-Cr alloys and the ternary alloys with nickel Fe-Cr(0–20 wt %)-Ni(5–15 wt %). In the four-component alloys Fe-Cr(0–20 wt %)-Ni(5–20 wt %)-X with $X = \text{Nb, V, W, Mo}$ the C_{11} are close to corresponding Fe-Cr(0–20 wt %)-Ni(5–20 wt %) alloys, only the Al significantly reduces the values of C_{11} . Since both Al and Ni simultaneously lower the elastic constant C_{11} , the Fe-Cr(0–20 wt %)-Ni(20 wt %)-Al(2.5–5.0 wt %) alloys have the lowest C_{11} . Thus the main trends are as follows: chromium increases C_{11} , nickel and aluminum decrease it.

The decrease of the elastic constant C_{11} in Al-containing alloys can be associated with an increase of the lattice parameter, which weakens the direct overlap of the orbitals of interacting atoms. In the case of Ni-containing alloys, the decrease of C_{11} can be caused by a decrease of the spatial

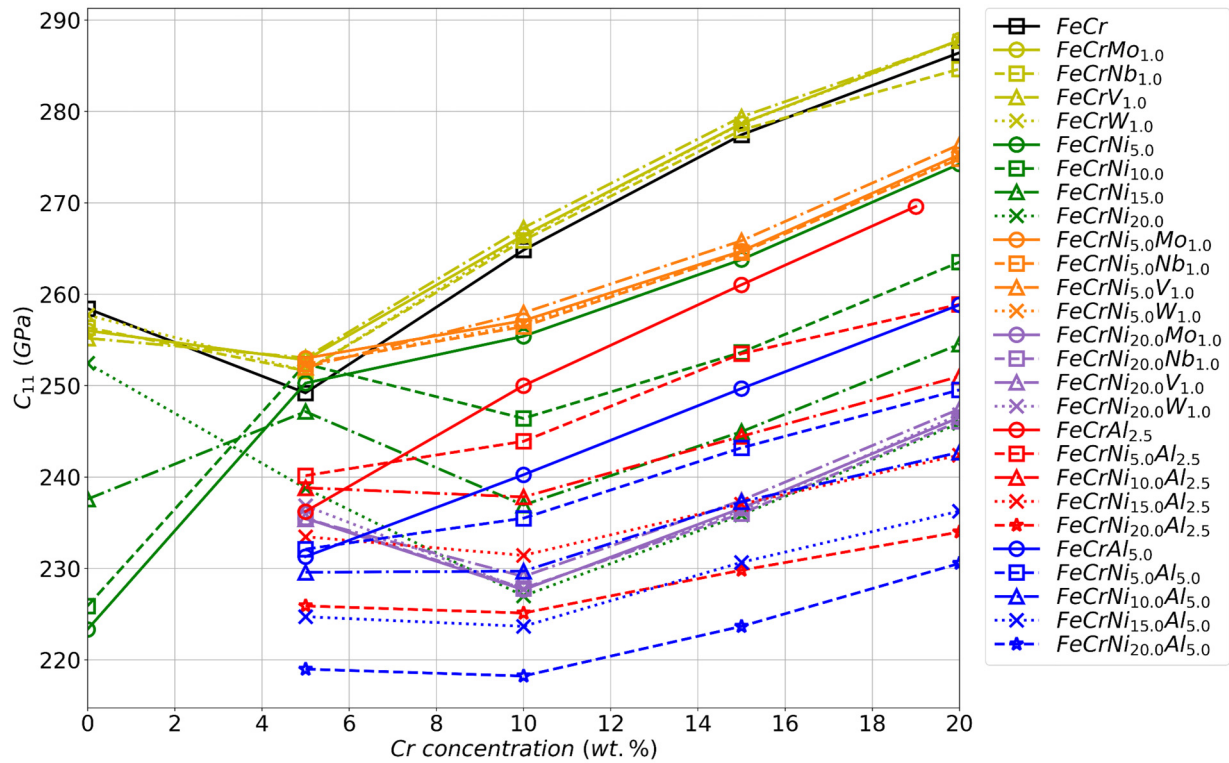


FIG. 7. Effect of multicomponent alloying on elastic constant C_{11} of bcc Fe-Cr-based alloys.

extent of $3d$ orbitals with an increase in the atomic number in the series of $3d$ elements.

The elastic constant C_{12} is related to the shear stress in the (110) plane along the (100) direction. The calculated values of

C_{12} are summarized in Fig. 8. For the C_{12} elastic constant of the binary Fe-Cr alloy one sees a well-developed minimum at $\sim 5\%$ Cr. Alloying with Nb, V, W, or Mo slightly increases the C_{12} . The addition of nickel also increases C_{12} , while

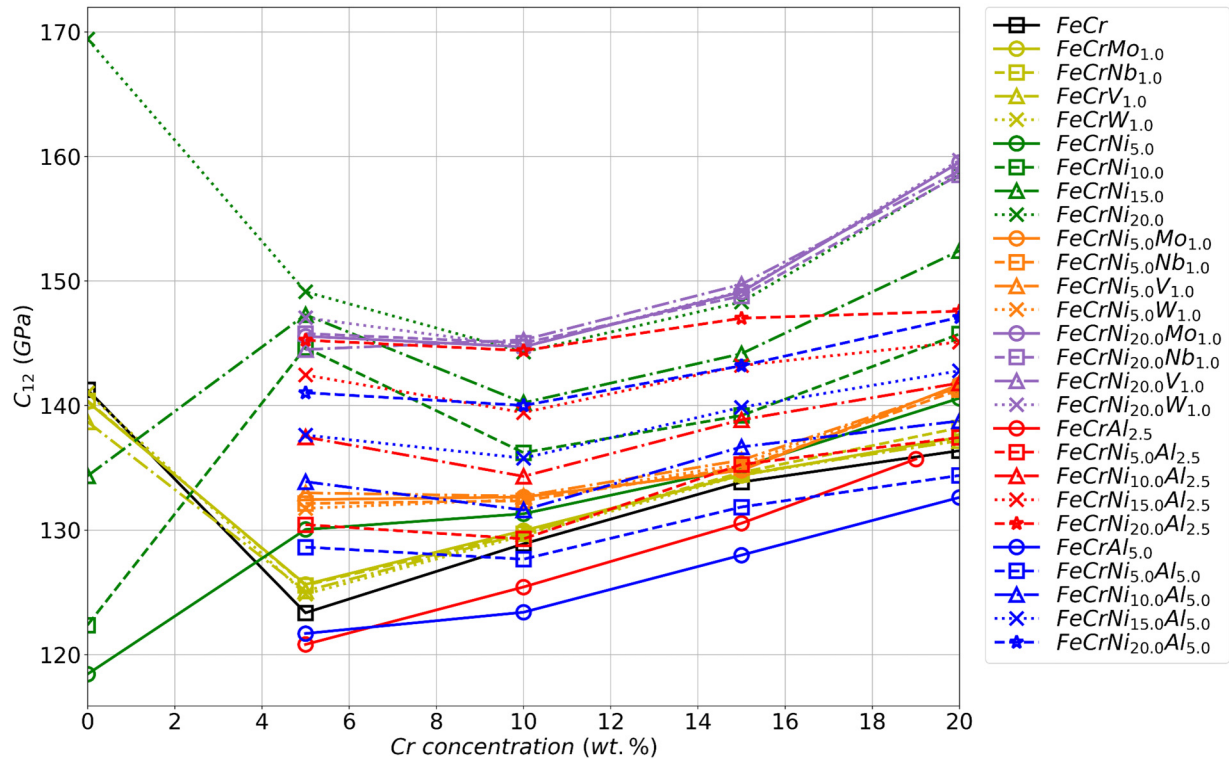


FIG. 8. Effect of multicomponent alloying on elastic constants C_{12} of bcc Fe-Cr-based alloys.

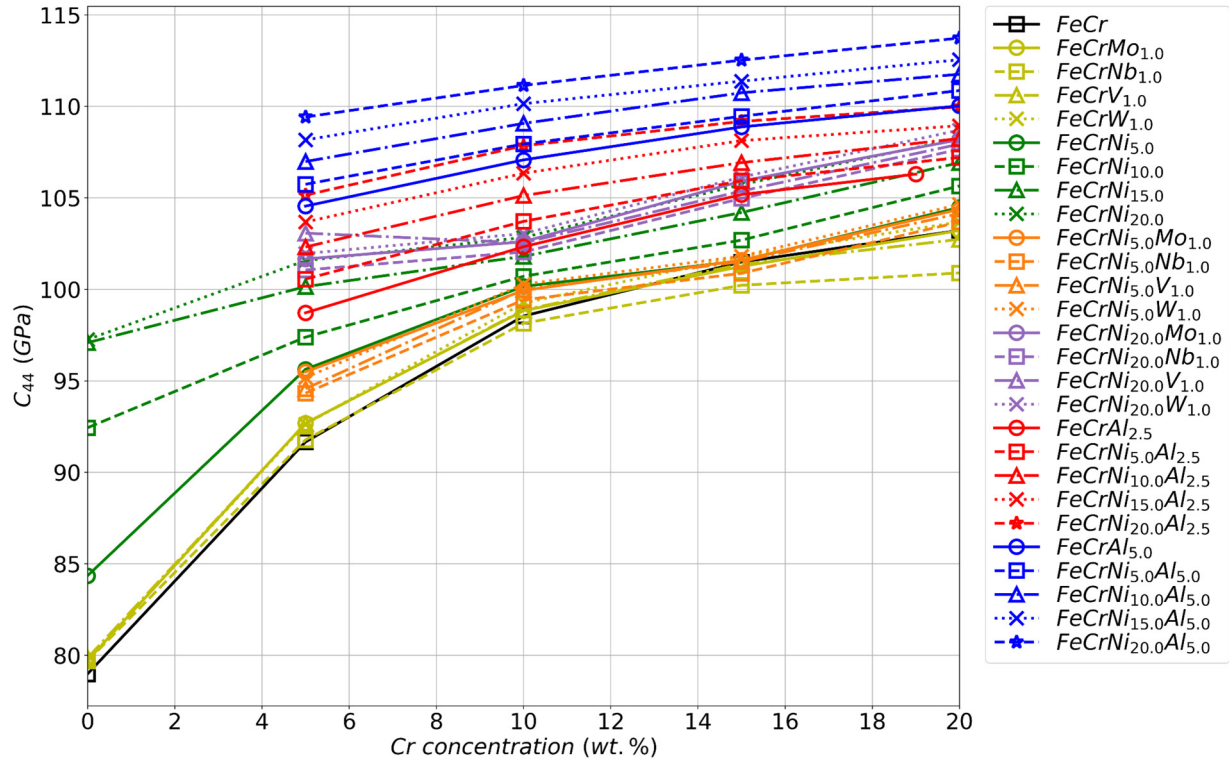


FIG. 9. Effect of multicomponent alloying on C_{44} elastic constant of bcc Fe-Cr-based alloys.

aluminum has the opposite effect. Note that the nonmonotonic behavior of C_{12} vs x_{Cr} can still be observed. The addition of Al decreases C_{12} , and an increase of Al concentration strengthens this effect. For all the studied alloys there is a minimum in the C_{12} elastic constant at $x_{Cr} \sim 10$ wt%, and the lowest value of the minimum corresponds to alloys containing 20 wt % Ni. Thus chromium and nickel increase C_{12} , while Al reduces it.

The elastic constant C_{44} shown in Fig. 9 is related to shear stress in the (010) plane and along the $\langle 100 \rangle$ direction. The values of the C_{44} for the binary Fe-Cr system monotonously increase with chromium concentration. The addition of 1 wt % Nb, V, W, or Mo does not have a significant effect on the values and behavior of C_{44} in the alloys. The slight decrease of C_{44} is detected only for the Fe-Cr(10–20 wt %)-Nb(1 wt %) alloys. On the other hand, alloying with Ni and Al provides stronger impact and leads to the increase of the elastic constant C_{44} . In the four-component alloys Fe-Cr(0–20 wt %)-Ni(5–20 wt %)-Al(2.5–5 wt %), only aluminum concentration significantly affects C_{44} , leading to their high values in the Fe-Cr(0–20 wt %)-Ni(20 wt %)-Al(5.0 wt %) alloys.

Thus we see that in general the studied alloying elements increase C_{44} , and aluminum has the strongest impact on the elastic constant. Considering the electronic DOS in Fig. 6, one can see a decrease in two peaks formed by Fe e_g states in the majority-spin channel with an energy of the order of -0.3 Ry and Cr e_g states in the minority-spin channel with an energy ~ -0.2 Ry in Al-containing alloys. This indicates that the atomic bonding becomes more directional, which is reflected in the increase of C_{44} .

Finally, it should be noted that all the studied alloys are mechanically stable, since the stability criteria for cubic crystals

are fulfilled:

$$C_{44} > 0, \quad C_{11} > |C_{12}|, \quad C_{11} + 2C_{12} > 0.$$

E. Polycrystalline elastic moduli

Figure 10 summarizes the calculated bulk moduli B of multicomponent bcc Fe-Cr-based alloys. The concentration dependence of the bulk moduli of the binary Fe-Cr alloys has a minimum at $x_{Cr} \sim 5$ wt%, in agreement with earlier calculations [46] and experiment [14]. In Ref. [5] it has been associated with a change of the Fermi surface topology. The addition of 1% V, Nb, W, or Mo slightly increases B compared to Fe-Cr alloys. The concentration dependences of the Ni-containing alloys are nonmonotonous. For the ternary alloys with aluminum the B are lower compared to the ternary alloys with nickel. The higher the Al content the lower the bulk modulus. In the four-component Fe-Cr(0–20 wt %)-Ni(5–20 wt %)-X alloys ($X = V, Nb, W, Mo$), B is close to the corresponding ternary alloys Fe-Cr(0–20 wt %)-Ni(5–20 wt %). For Al-containing four-component alloys the curves are close to Fe-Cr(0–20 wt %)-Al(2.5–5 wt %) alloys. We notice that the higher the Ni content the lower the curve “ B vs x_{Cr} ” is located, and the minimum at $x_{Cr} \sim 10$ wt% becomes more distinct.

The concentration dependences of the bulk moduli for alloys containing nickel and aluminum have an inverse correlation with the lattice parameters: the largest values of the lattice parameters for Fe-Cr(0–20 wt %)-Ni(5 wt %)-Al(5 wt %) alloys correspond to the lowest values of the bulk moduli. This can be explained considering the volume, which is available for the gas of valence electrons. It corresponds to the region between the core radius and the muffin-tin sphere and

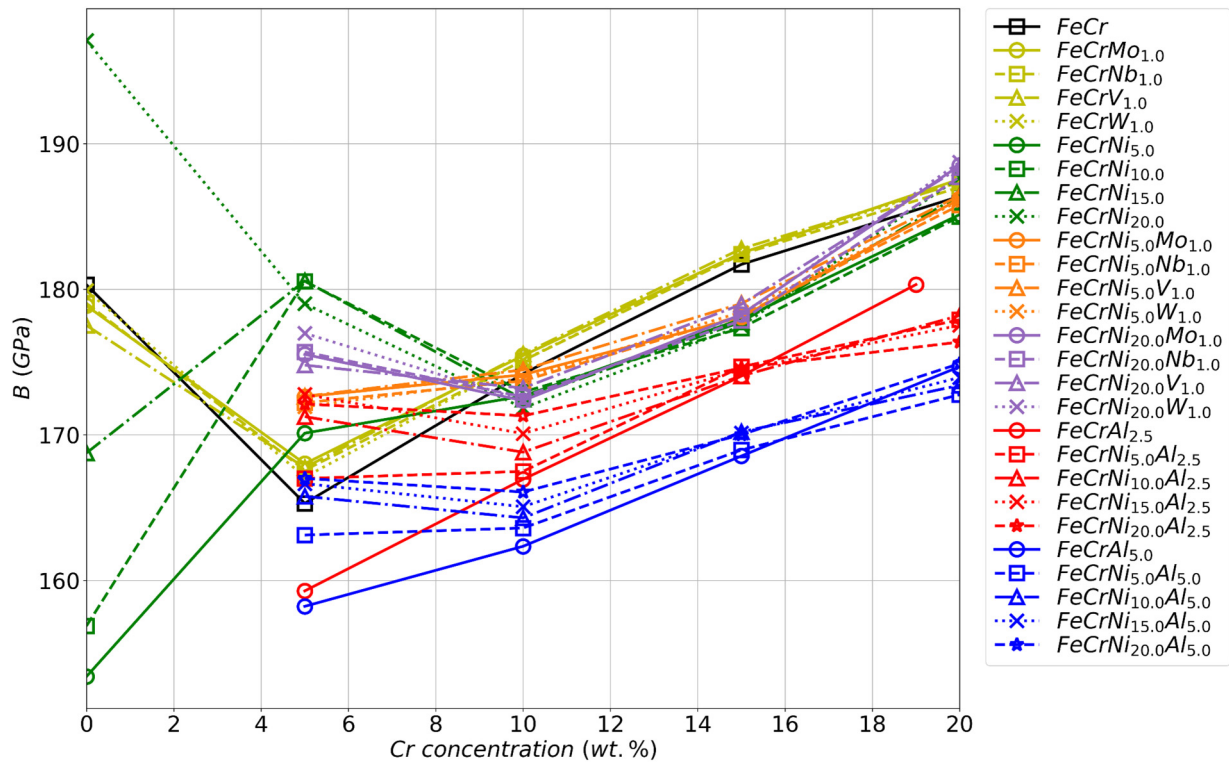


FIG. 10. Effect of multicomponent alloying on bulk moduli B of bcc Fe-Cr-based alloys.

effectively increases with the increase of the lattice parameter. This increases the compressibility of the crystal and reduces the bulk modulus [47].

In Figs. 11 and 12 we plot the calculated values of the Young’s modulus E and shear modulus G , respectively. The E modulus measures of the stiffness of a solid, while the

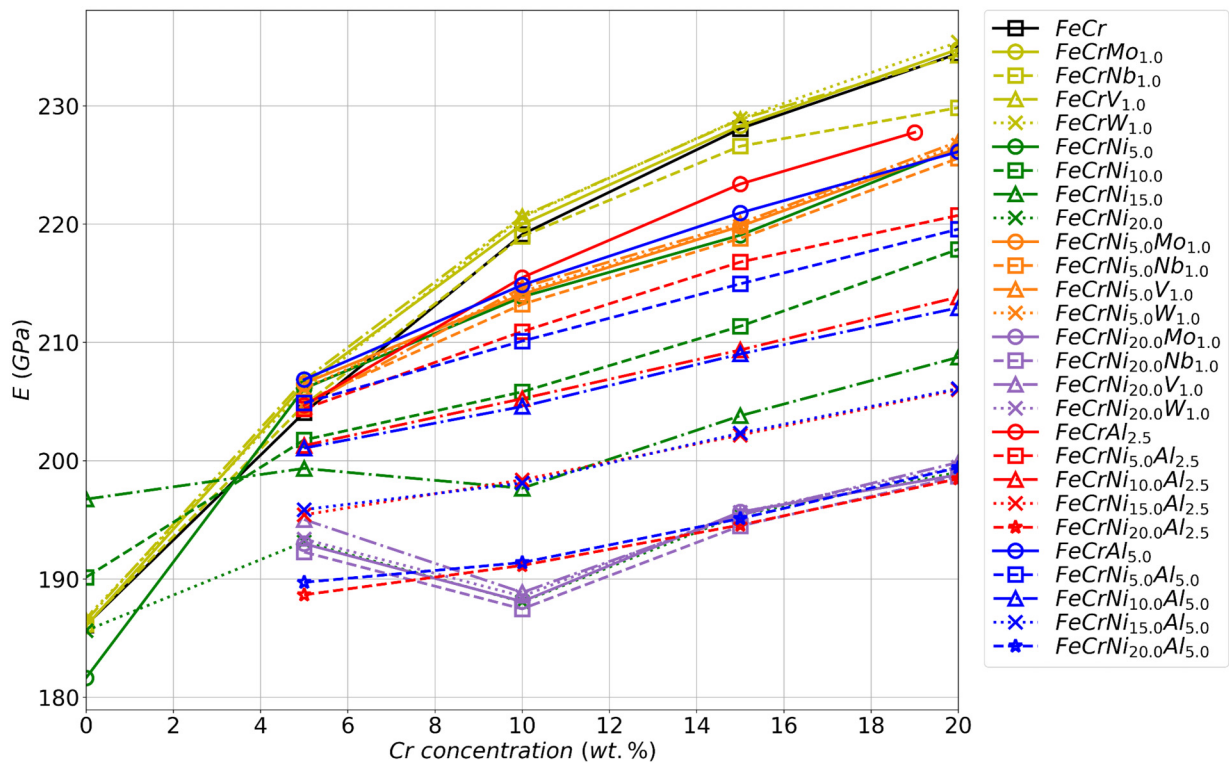


FIG. 11. Effect of multicomponent alloying on Young’s modulus E of bcc Fe-Cr-based alloys.

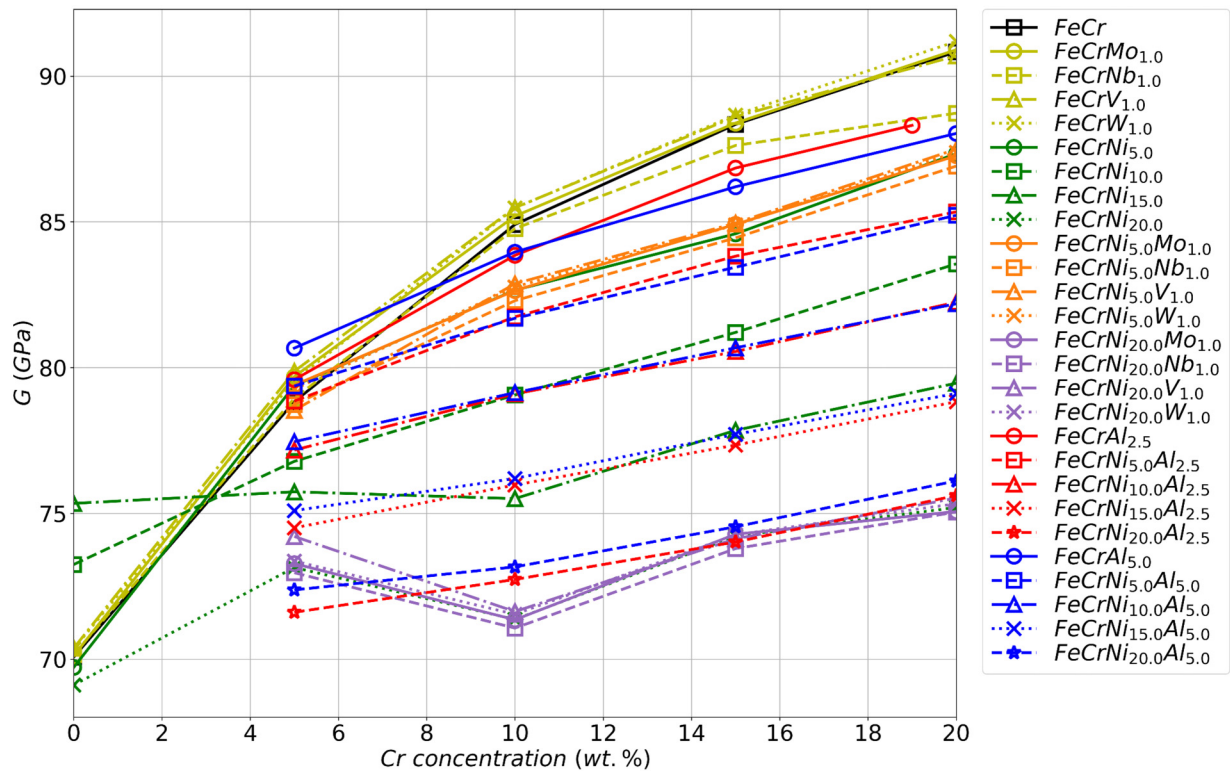


FIG. 12. Effect of multicomponent alloying on shear modulus G of bcc Fe-Cr-based alloys.

shear modulus represents the ability of materials to withstand shape changes, which in some models is associated with an ability of the material to resist the elastic strain. In addition, there are models that correlate G with the hardness of the material.

The values of the Young's modulus E and shear modulus G show very similar trends. The binary Fe-Cr and ternary Fe-Cr- X alloys with $X = 1\%$ Nb, V, W, Mo have the higher values of E and G . Aluminum in ternary alloys also increases the moduli. On the contrary, the addition of Ni reduces the E and G . In the four-component alloys Fe-Cr(0–20 wt %)-Ni(5–20 wt %)-Al(2.5–5.0 wt %), aluminum is not able to fully compensate the drop in E and G due to alloying with Ni; therefore their values are close to the corresponding ternary alloys with nickel. However, the influence of chromium on the moduli remains dominant in the multicomponent alloys: they increase with Cr concentration, though lying below the E and G values of the binary Fe-Cr alloys.

Finally, to analyze how the multicomponent alloying affects the mechanical properties of the studied materials we considered two phenomenological relations: the Cauchy pressure $P_C = (C_{12} - C_{44})$ [47] and the G/B ratio [48], which allows one to assess the tendency to brittleness in materials. If $G/B > 0.5$ and $P_C < 0$, the alloy is expected to be brittle with predominantly covalent nature of chemical bonding. On the contrary, in case of $G/B < 0.5$ and $P_C > 0$ the material is expected to be ductile with a metallic type of bonding. Of course, the two criteria should be used with care. In particular, it has been shown that the correlation between them and brittleness or ductility of bcc Fe-Ni and Fe-Mn alloys is not perfect when the elastic anisotropy is substantial [49].

Zhang *et al.* demonstrated that the brittle-to-ductile transitions in $\text{Al}_x\text{CrMnFeCoNi}$ high-entropy alloys is better described in terms of the Cauchy pressure and Pugh ratio when they accounted for the strong elastic anisotropy in the alloys [50]. Still, discussing the qualitative trends of the G/B ratio and P_C observed upon the multicomponent alloying of the bcc Fe-Cr system is of interest. Note that we are only discussing the trends qualitatively, comparing the calculated parameters between different systems.

The calculated values of the G/B and P_C show similar behavior; therefore in the main text of the article we analyze the former (Fig. 13). P_C values are plotted in Fig. S5 in the Supplemental Material [24]. The G/B ratio in the binary Fe-Cr alloys increases rapidly up to 5 wt % Cr followed by a substantially slower increase with further increase of Cr concentration. Though the calculated values are slightly below the experimental data (see Fig. 2), the alloys could be classified as the ductile materials with a metallic type of bonding. In most cases the multicomponent alloying does not change this conclusion. We do not observe significant changes in the G/B ratio with addition of 1 wt % Nb, V, W, or Mo. However, W or Mo can slightly enhance G/B in the case of high Cr content. In Fe-Cr(0–20 wt %)-Ni(5 wt %) alloys the dependence of the G/B ratio has a weak maximum at $x_{\text{Cr}} \sim 10\text{wt}\%$. In the ternary alloys with 10, 15, and 20 wt % Ni the concentration dependencies are nonmonotonous, and one observes a weak decrease of the G/B ratio at $x_{\text{Cr}} > 10\text{wt}\%$. The curves are below that of the binary Fe-Cr alloy, and the lowest G/B ratios are observed at 20 wt % Ni. The addition of 2.5–5 wt % Al substantially increases the G/B ratio, and among all the studied alloys the largest values of G/B ratios are calculated

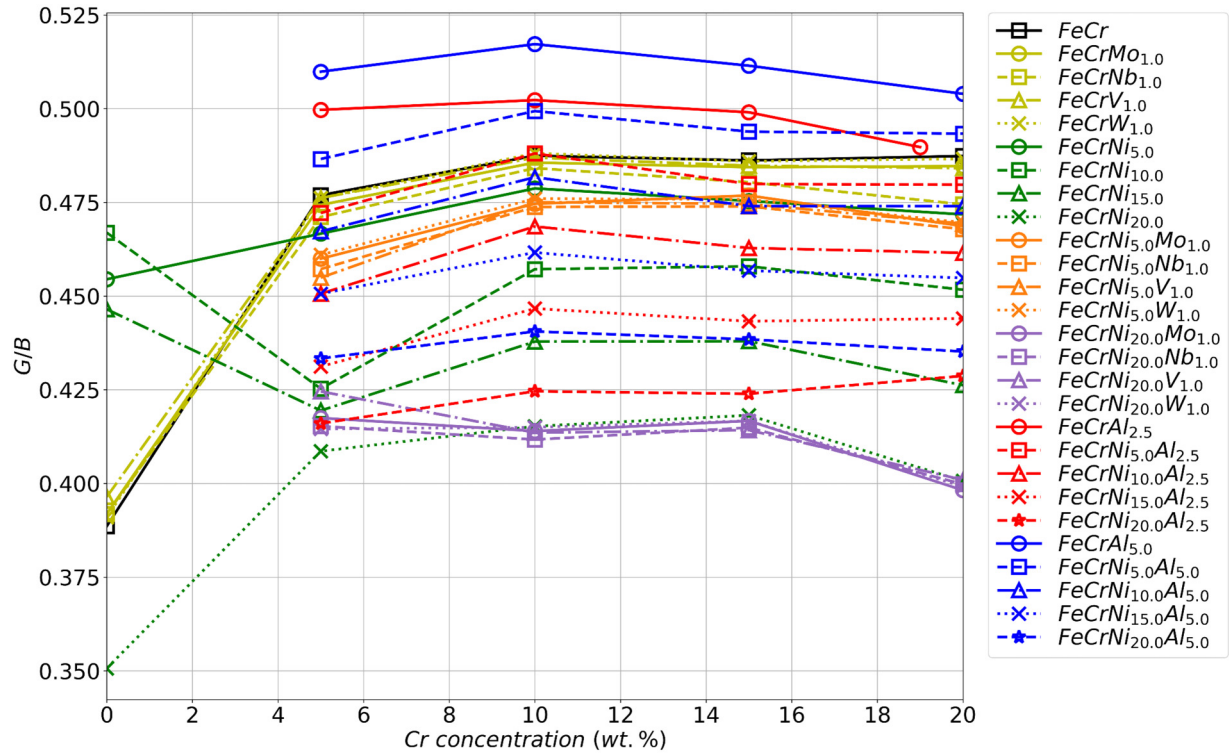


FIG. 13. Effect of multicomponent alloying on G/B parameter of Fe-Cr alloys.

for Fe-Cr(0–20 wt %)-Al(5 wt %). The four-component alloys Fe-Cr(0–20 wt %)-Ni(5 wt %)-X(1 wt %) where $X = \text{Nb, V, W, Mo}$ have approximately the same G/B as the ternary Fe-Cr(0–20 wt %)-Ni(5 wt %) systems. For the four-component alloys with 2.5–5 wt % Al the G/B ratio becomes higher than in the corresponding ternary Ni-containing alloys, but it is still lower compared to Ni-free and Al-containing ternary alloys. Thus nickel somewhat compensates the impact of aluminum. For high Cr concentrations, the alloys with 1% Nb, V, W, Mo have G/B values close to Fe-Cr(0–20 wt %)-Ni(20 wt %) alloys. Also, the aluminum-containing alloys Fe-Cr(0–20 wt %)-Ni(20 wt %)-Al(2.5–5 wt %) have lower G/B compared to Fe-Cr alloys and nickel-free alloys with aluminum.

A decrease in the G/B parameter (and an increase in P_C) for Fe-Cr(0–20 wt %)-Ni(10–20 wt %), Fe-Cr(0–20 wt %)-Ni(20 wt %)-X(1 wt % Nb, V, W, Mo) and Fe-Cr(0–20 wt %)-Ni(15–20 wt %)-Al(2.5–5 wt %) alloys indicate that the metallic type of atomic bonding is dominant in these systems. Herewith, an increase of elastic constant C_{44} (Fig. 9) indicates the presence of a covalent component in the bonding. An increase in the G/B ratio (and a decrease in P_C) for the ternary alloys with aluminum Fe-Cr(0–20 wt %)-Al(2.5–5 wt %) and Fe-Cr(0–20 wt %)-Ni(5 wt %)-Al(5 wt %) indicates that the fraction of the covalent components in the bonding increases, which enhances the tendency to form directional bonds. The same conclusion was made from analysis of the density of states (Fig. 6). The presence of covalent components increases shear resistance of the materials, which is fully reflected in the maximum values of the elastic constant C_{44} in the studied alloys. This is also reflected in the high values of the E and G moduli.

According to the studied criteria, the presence of nickel in alloys with concentrations above 5 wt % should significantly increase their ductility. This can be explained by the fact that alloying with the nickel increases the density of valence electrons, while increasing chromium content makes them more delocalized. Indeed, from the electronic DOS shown in Fig. 6 one can see that for nickel-containing alloys the DOS at the Fermi level increases due to e_g Ni electrons. At the same time, the peak in the minority-spin channel is smeared out in a range -0.1 to -0.2 Ry due to Ni t_{2g} electrons, which increases the metallicity of the system and could lead to the improved ductility.

Summarizing this section, we see that our calculations predict that the presence of aluminum in the studied alloys should give the highest embrittlement effect, while the ductility of Fe-Cr alloys can be improved by additions of nickel. Therefore a combination of nickel and aluminum alloying in Fe-Cr alloys makes it possible to optimize the G/B ratio as well as the phase stability of the multicomponent bcc Fe-Cr-based alloys, as discussed in Sec. IV B.

V. CONCLUSION

In this work we studied the effect of multicomponent alloying on the thermodynamic and mechanical properties of the bcc Fe-Cr-based solid solutions. We performed first-principles calculations of the lattice parameters, mixing enthalpies, magnetic moments, and elastic constants of disordered alloys containing up to 20 wt % of Cr and Ni, as well as small concentrations of other alloying elements, Mo, Al, W, V, and Nb. The calculations show that Nb, V, W, Mo, and Al increase the lattice parameter, while nickel (in alloys with $x_{\text{Cr}} > 5\text{wt}\%$)

and chromium (also for $x_{\text{Cr}} > 5\text{wt}\%$) decrease the lattice parameter. In the four-component alloys containing both Ni and Al, the impact of the latter is stronger and the lattice parameter increases.

Calculations of the mixing enthalpy show that the addition of aluminum to the binary Fe-Cr alloys provides the highest stabilizing effect, while nickel destabilizes the alloys. The alloying with 1 wt % of Nb, W, or Mo to ternary Fe-Cr(0–20 wt %)-Ni(5–20 wt %) alloys decreases the stability of the four-component alloys. Considering the magnetic properties of the studied multicomponent alloys, we observe a correlation between the mixing enthalpy and the magnitude of the local moment on Fe atoms in the alloys: the elements that decrease the Fe magnetic moment increase the stability of the respective alloys and vice versa.

From calculations of the single-crystal elastic constants, we conclude that chromium increases the elastic constant C_{11} while nickel and aluminum decrease it. Moreover, chromium and nickel increase C_{12} values, while Al decreases it. All alloying elements increase the C_{44} , and the effect is strongest upon the alloying with Al.

According to our calculations and phenomenological criteria linking the elastic moduli and the mechanical properties

of materials, the Fe-Cr-based alloys should belong to the class of ductile materials with a metallic type of bonding. Multicomponent alloying practically does not change this conclusion, except for Al-containing alloys with a narrow range of Cr concentrations (10–16 wt %). The alloying with aluminum is predicted to cause the embrittlement of the material. On other hand, nickel improves the ductility of the alloys. Therefore, the combination of the nickel and aluminum alloying makes it possible to vary the G/B parameter controlling the brittleness of the multicomponent alloys. We conclude that alloys in the Fe-Cr-Ni-Al system are predicted to simultaneously show significant increase of their thermodynamic stability and ductility without significant degradation of the mechanical properties: their E and G moduli are within the range of the binary low-chromium steels.

ACKNOWLEDGMENTS

This work was carried out with the financial support of the Ministry of Science and Higher Education of the Russian Federation (Grant No. PNIER RFMEFI60719X0323).

-
- [1] C. Cabet, F. Dalle, E. Gaganidze, J. Henry, and H. Tanigawad, Ferritic-martensitic steels for fission and fusion applications, *J. Nucl. Mater.* **523**, 510 (2019).
- [2] P. Olsson, I. A. Abrikosov, and J. Wallenius, Electronic origin of the anomalous stability of Fe-rich bcc Fe-Cr alloys, *Phys. Rev. B* **73**, 104416 (2006).
- [3] T. P. C. Klaver, R. Drautz, and M. W. Finnis, Magnetism and thermodynamics of defect-free Fe-Cr alloys, *Phys. Rev. B* **74**, 094435 (2006).
- [4] A. V. Ruban, P. A. Korzhavyi, and B. Johansson, First-principles theory of magnetically driven anomalous ordering in bcc Fe-Cr alloys, *Phys. Rev. B* **77**, 094436 (2008).
- [5] P. A. Korzhavyi, A. V. Ruban, J. Odqvist, J.-O. Nilsson, and B. Johansson, Electronic structure and effective chemical and magnetic exchange interactions in bcc Fe-Cr alloys, *Phys. Rev. B* **79**, 054202 (2009).
- [6] A. V. Ponomareva, A. V. Ruban, O. Yu. Vekilova, S. I. Simak, and I. A. Abrikosov, Effect of pressure on phase stability in Fe-Cr alloys, *Phys. Rev. B* **84**, 094422 (2011).
- [7] F. Ducastelle and F. Gautier, Generalized perturbation theory in disordered transitional alloys: Applications to the calculation of ordering energies, *J. Phys. F: Met. Phys.* **6**, 2039 (1976).
- [8] A. T. Aldred, B. D. Rainford, J. S. Kouvel, and T. J. Hicks, Ferromagnetism in iron-chromium alloys, II. Neutron scattering studies, *Phys. Rev. B* **14**, 228 (1976).
- [9] I. Mirebeau, M. Hennier, and G. Parette, First Measurement of Short-Range-Order Inversion as a Function of Concentration in a Transition Alloy, *Phys. Rev. Lett.* **53**, 687 (1984).
- [10] M. Yu. Lavrentiev, R. Drautz, D. Nguyen-Manh, T. P. C. Klaver, and S. L. Dudarev, Monte Carlo study of thermodynamic properties and clustering in the bcc Fe-Cr system, *Phys. Rev. B* **75**, 014208 (2007).
- [11] V. I. Razumovskiy, A. V. Ruban, and P. A. Korzhavyi, Effect of Temperature on the Elastic Anisotropy of Pure Fe and Fe_{0.9}Cr_{0.1} Random Alloy, *Phys. Rev. Lett.* **107**, 205504 (2011).
- [12] H. Zhang, G. Wang, M. P. J. Punkkinen, S. Hertzman, B. Johansson, and L. Vitos, Elastic anomalies in Fe-Cr alloys, *J. Phys.: Condens. Matter.* **25**, 195501 (2013).
- [13] H. Zhang, B. Johansson, and L. Vitos, Ab initio calculations of elastic properties of bcc Fe-Mg and Fe-Cr random alloys, *Phys. Rev. B* **79**, 224201 (2009).
- [14] G. Speich, A. Schwoeble, and W. Leslie, Elastic constants of binary iron-base alloys, *Metall. Trans.* **3**, 2031 (1972).
- [15] J. S. Wróbel, D. Nguyen-Manh, M. Yu. Lavrentiev, M. Muzyk, and S. L. Dudarev, Phase stability of ternary fcc and bcc Fe-Cr-Ni alloys, *Phys. Rev. B* **91**, 024108 (2015).
- [16] A. V. Ponomareva, A. V. Ruban, B. O. Mukhamedov, and I. A. Abrikosov, Effect of multicomponent alloying with Ni, Mn and Mo on phase stability of bcc Fe-Cr alloys, *Acta Mater.* **150**, 117 (2018).
- [17] X. Li, X. Li, S. Schönecker, R. Li, J. Zhaoa, and L. Vitos, Understanding the mechanical properties of reduced activation steels, *Mater. Des.* **146**, 260 (2018).
- [18] L. Vitos, *Computational Quantum Mechanics for Materials Engineers: The EMTO Method and Applications* (Springer-Verlag, London, 2007), pp. 83–101.
- [19] L. Vitos, I. A. Abrikosov, and B. Johansson, Anisotropic Lattice Distortions in Random Alloys from First-Principles Theory, *Phys. Rev. Lett.* **87**, 156401 (2001).
- [20] J. Kollar, L. Vitos, and H. L. Skriver, *Electronic Structure and Physical Properties of Solids: The Uses of the LMTO Method* (Springer-Verlag, Berlin, 2000), pp. 85–113.
- [21] J. P. Perdew and Y. Wang, Accurate and simple analytic representation of the electron-gas correlation energy, *Phys. Rev. B* **45**, 13244 (1992).
- [22] J. P. Perdew, K. Burke, and M. Ernzerhof, Generalized Gradient Approximation Made Simple, *Phys. Rev. Lett.* **77**, 3865 (1996).

- [23] A. V. Ruban and I. A. Abrikosov, Configurational thermodynamics of alloys from first principles: Effective cluster interactions, *Rep. Prog. Phys.* **71**, 046501 (2008).
- [24] See Supplemental Material at <http://link.aps.org/supplemental/10.1103/PhysRevMaterials.4.094406> for information on workflow for high-throughput calculations, local magnetic moments and Cauchy pressure for alloys considered in this study.
- [25] A. Zunger, S.-H. Wei, L. G. Ferreira, and J. E. Bernard, Special Quasirandom Structures, *Phys. Rev. Lett.* **65**, 353 (1990).
- [26] P. E. Blöchl, Projector augmented-wave method, *Phys. Rev. B* **50**, 17953 (1994).
- [27] G. Kresse and J. Hafner, Ab initio molecular dynamics for open-shell transition metals, *Phys. Rev. B* **48**, 13115 (1993).
- [28] G. Kresse and J. Furthmüller, Effective interactive schemes for ab initio total-energy calculations using a plane-wave basis set, *Phys. Rev. B* **54**, 11169 (1996).
- [29] M. Methfessel and A. T. Paxton, High-precision sampling for Brillouin-zone integration in metals, *Phys. Rev. B* **40**, 3616 (1989).
- [30] Q.-M. Hu, S. Lu, and R. Yang, Elastic stability of β -Ti under pressure calculated using a first-principles plane-wave pseudopotential method, *Phys. Rev. B* **78**, 052102 (2008).
- [31] F. Birch, Finite elastic strain of cubic crystals, *Phys. Rev.* **71**, 809 (1947).
- [32] H. L. Zhang, S. Lu, M. P. J. Punkkinen, Q.-M. Hu, B. Johansson, and L. Vitos, Static equation of state of bcc iron, *Phys. Rev. B* **82**, 132409 (2010).
- [33] C. Varvenne, F. Bruneval, M.-C. Marinica, and E. Clouet, Point defect modeling in materials: Coupling ab initio and elasticity approaches, *Phys. Rev. B* **88**, 134102 (2013).
- [34] P.-W. Ma and S. L. Dudarev, CALANIE: Anisotropic elastic correction to the total energy, to mitigate the effect of periodic boundary conditions, *Comp. Phys. Comm.* **252**, 107130 (2020).
- [35] I. A. Abrikosov, Yu. H. Vekilov, P. A. Korzhavyi, A. V. Ruban, and L. E. Shilkrot, Ab initio calculations of the electronic topological transition in Li-Mg alloys, *Solid State Commun.* **83**, 867 (1992).
- [36] A. V. Ruban and H. L. Skriver, Screened Coulomb interactions in metallic alloys, I. Universal screening in the atomic-sphere approximation, *Phys. Rev. B* **66**, 024201 (2002).
- [37] A. V. Ruban, S. I. Simak, P. A. Korzhavyi, and H. L. Skriver, Screened Coulomb interactions in metallic alloys, II. Screening beyond the single-site and atomic-sphere approximations, *Phys. Rev. B* **66**, 024202 (2002).
- [38] I. A. Abrikosov and B. Johansson, Applicability of the coherent approximation in the theory of random alloys, *Phys. Rev. B* **57**, 14164 (1998).
- [39] I. A. Abrikosov, A. M. N. Niklasson, S. I. Simak, B. Johansson, A. V. Ruban, and H. L. Skriver, Order-N Green's Function Technique for Local Environment Effects in Alloys, *Phys. Rev. Lett.* **76**, 4203 (1996).
- [40] I. A. Abrikosov, S. I. Simak, B. Johansson, A. V. Ruban, and H. L. Skriver, Locally self-consistent Green's function approach to electronic structure problem, *Phys. Rev. B* **56**, 9319 (1997).
- [41] O. E. Peil, A. V. Ruban, and B. Johansson, Self-consistent supercell approach to alloys with local environment effects, *Phys. Rev. B* **85**, 165140 (2012).
- [42] M. Ekholm and I. A. Abrikosov, Structural and magnetic ground-state properties of γ -FeMn alloys from ab initio calculations. *Phys. Rev. B* **84**, 104423 (2011).
- [43] G. D. Preston, An x-ray examination of iron-chromium alloys, *Philos. Mag.* **3**, 419 (1932).
- [44] W. B. Pearson, *A Handbook of Spacings and Structures of Metals and Alloys*, Vol. 4 (Pergamon, Oxford, 1958), pp. 532–534.
- [45] D. R. Lide, *Handbook of Chemistry and Physics*, 85th ed. (CRC Press, Boca Raton, FL, 2004).
- [46] V. I. Razumovskiy, A. V. Ruban, and P. A. Korzhavyi, First-principles study of elastic properties of Cr- and Fe-rich Fe-Cr alloys, *Phys. Rev. B* **84**, 024106 (2011).
- [47] D. G. Pettifor, *Bonding and Structure of Molecules and Solids* (Clarendon Press, Oxford, 1995).
- [48] S. F. Pugh, Relations between the elastic moduli and the plastic properties of polycrystalline pure metals, *Philos. Mag. Ser.* **745**, 823 (1954).
- [49] G. Wang, S. Schönecker, S. Hertzman, Q. M. Hu, B. Johansson, S. K. Kwon, and L. Vitos, Ab initio prediction of the mechanical properties of alloys: The case of Ni/Mn-doped ferromagnetic Fe, *Phys. Rev. B* **91**, 224203 (2015).
- [50] H. Zhang, X. Sun, and S. Lu, Z. Dong, X. Ding, Y. Wang, and L. Vitos, Elastic properties of $\text{Al}_x\text{CrMnFeCoNi}$ ($0 \leq x \leq 5$) high-entropy alloys from ab initio theory, *Acta Mater.* **155**, 12 (2018).